Electrodeposited and Sputtered Selective Coatings for Solar-to-Thermal Energy Conversion

Lizama-Tzec F.[1], Pérez-Espinoza R.[2], Vega-Poot A.[1], Herrera-Zamora D.[1], Becerril-González J.[1], Cetina-Dorantes M.[1], Rodriguez-Gattorno G.[1], Ares-Muzio O.[1], García-Valladares O.[3], Oskam G.[1]

[1]Departamento de Física Aplicada, Centro de Investigación y de Estudios Avanzados del IPN, Mérida, Yucatán, México.

[2]Módulo Solar S.A. de C.V., Calle 23 Este No. 3, Col. CIVAC, 62578, Jiutepec, Morelos, México.

[3]Instituto de Energías Renovables de la Universidad Nacional Autónoma de México (IER-UNAM), Privada Xochicalco s/n, 62580, Temixco, Morelos, México.

Abstract

In this work, we report on the deposition and characterization of selective coatings for solar-to-thermal energy conversion systems for applications of low to medium temperatures. Both sputtering and electrodeposition were used to deposit the layers of typical multilayer coatings. The completely electrodeposited selective films consist of an infrared reflecting nickel interlayer on stainless steel, and a black nickel solar absorber material. An alumina/molybdenum/alumina (AMA) multilayer absorber material was deposited by sputtering on stainless steel and copper with electrodeposited nickel (Cu/Ni). The optical properties of the films were studied as a function of the thermal treatment and were compared with similar selective coatings with sputtered alumina as antireflective coating. The films were thermally treated and characterized by reflectance spectroscopy, FESEM, DSC, XRD, profilometry and Raman measurements. Finally, we report on the scale-up of these films, and the results obtained on individual fin collectors showed that our selective coatings exhibit a performance close to the benchmark coating in the market.

Keywords: Electrodeposition, Sputter deposition, Solar-to-Thermal Energy Conversion,

1. Introduction

Selective coatings for solar thermal applications are usually obtained by sputtering or electrodeposition (Wackelgard, Ewa; Hultmark, 1998), (Wäckelgard, 1998), (Gogna and Chopra, 1979), (Nunes et al., 2018), (Manson and Brendel, 1982), (Patel et al., 1985), (Abbas, 2000), and a wide range of systems has been reported (Boström et al., 2004), (Boström et al., 2007), (Khatibani and Rozati, 2016). However, there are still many systems left to explore, in particular when combining sputter-deposited layers with electrodeposited layers in a single system. Also, within both the electrodeposition and sputter deposition methods, there are still many variables that may be evaluated to improve performance. The current market for selective coatings is dominated by coatings obtained by PVD (physical vapor deposition), but several companies that use electroplating are gradually obtaining a part of the market (Berner, 2016). Currently no company combines the advantages of electroplating with PVD technologies to have better coatings. In this work, we evaluated the performance and feasibility of obtaining a deposit based on electrodeposition of selective coatings and the application of antireflective coating by sputtering on stainless steel and copper, both for smaller area and for industrial size substrates. We have obtained selective coatings on copper and stainless steel and evaluated their optical properties and thermal stability. The main motivation is to determine the most suitable synthesis conditions for the scale-up towards functional pieces. The pieces have been applied in a single fin collector system, and the several coatings have been evaluated and compared against commercial Cu-TiNOX coating.

Selection and/or peer review under responsibility of Scientific Committee
doi:10.18086/eurosun.2020.06.07 Available at http://proceedings.ises.org

2. Experimental

For the films obtained by electroplating, a potentiostat-galvanostat Gamry Reference 3000 was used, employing stainless steel (AISI 304) pieces of 0.04 m x 0.06 m as substrate. The stainless steel was used to study the thermal performance of the black nickel absorber film. The stainless steel substrate was initially treated with a nickel strike bath under the conditions previously reported (Lizama-Tzec et al., 2014). The selective coating electrodeposition procedure for the bright nickel film was from a modified Watts bath at -50 A m^{-2} and the black nickel film was electrodeposited from a plating bath based on $NiCl_2$ and NaCl. The films were obtained by applying two pulses of 60 s at -26 A m^{-2} and 90 s at -14 A m^{-2}. The electrodeposition area was 0.0016 m^2. After black nickel electrodeposition, a thin film of 300 nm alumina was applied. For the deposition of alumina, the RF sputtering technique was used at 280 W; the chamber was evacuated to 1.3 x 10^{-3} Pa and an argon atmosphere was employed. Magnetron guns with targets of alumina were used to deposit the alumina coatings. The AMA deposition process was optimized on borosilicate glass (2.6 cm x 7.6 cm x 1 mm) and after that applied to stainless steel. These coatings are composed of 3 layers: Al_2O_3-Mo-Al_2O_3 from top to bottom. The alumina films (90 nm) and the Mo intermediate layer (10 nm) were deposited using RF-sputtering at 0.93 Pa of argon pressure and a power of 280 W. The samples were subjected to thermal treatment processes in a muffle furnace (Thermo Scientific, model FB1315M), consisting in one heating cycle for the stainless steel samples at 250 ºC for 200 hours at a heating ramp of 0.16 ºC s^{-1} for substrates. The selective coatings were obtained under the conditions and treatments listed in Table 1.

Tab. 1: Methods used for the preparation and thermal treatments of selective coatings prepared on this work.

Sample	Current Density (A m^{-2})	Time (s)	Treatment Temperature (ºC)	Time (h)
SS/Ni/NB	-26/-14	60/90	N/A	N/A
SS/Ni/NB thermally treated	-26/-14	60/90	250	200
SS/Ni/NB/Alumina	-26/-14	60/90	N/A	N/A
SS/Ni/NB/Alumina-thermally treated	-26/-14	60/90	250	200
SS/AMA	N/A	N/A	400	2

The selective coatings were characterized by relative total reflectance spectroscopy (Shimadzu Corporation, 2013) using a UV-Vis spectrophotometer (Avantes, model Avaspec 2048, in the wavelength range: 0.3 to 2.5 μm), and an infrared spectrometer (Avantes, model Avaspec-Nir 256-2.5), both with an integrating sphere (Avantes, model 50-Ls-HAL). For the UV-VIS-NIR measurements, the AVANTES WS-2 white reflective tile, consisting of a white, diffuse, high-grade PTFE material, was used as the reference. The reflectance spectra obtained in the range of 2.5 to 15 μm was obtained with an FTIR spectrometer (Perkin Elmer, Frontier NIR/MIR model), equipped with an integrating sphere (PICO, Integrat IR model), and a gold standard was used as the reference. The solar absorptance was determined by weighting the reflection spectrum against the solar radiation spectrum ASTM G173-0329, using equation (1). To approximate the thermal emittance at maximum real operating conditions of the devices, the emittance was calculated using T= 250 ºC in equation (2). To determine the thermal emittance, the reflection of the coatings was measured by weighting the reflection spectrum against the blackbody radiation at 250 ºC. The corresponding equations are:

$$\alpha = \frac{\int_{0.3}^{2.5} I_{SUN}(\lambda)\,[1-\rho(\lambda)]d\lambda}{\int_{0.3}^{2.5} I_{SUN}(\lambda)} \qquad \text{(eq. 1)}$$

$$\varepsilon = \frac{\int_{2.5}^{15} I_b(\lambda)\,[1-\rho(\lambda)]d\lambda}{\int_{2.5}^{15} I_b(\lambda)} \qquad \text{(eq. 2)}$$

where ρ(λ) is the wavelength dependent reflectance, and the black body radiation as a function of wavelength and temperature is given by $I_b(\lambda,T) = c_1/\left\{\lambda^5\left[e^{\left(\frac{c_2}{\lambda T}\right)}-1\right]\right\}$ with $c_1 = 3.743\text{x}10^{-16}$ W m^2 and $c_2 = 1.4387\text{x}10^{-2}$ m K.

The wavelength limits in the integral are chosen according to our experimental capabilities. The electrodeposited films were studied by field emission scanning electron microscopy (FESEM) (JEOL JSM-7600F), X-ray diffraction (XRD) was performed using a Siemens D-5000 for the analysis of the selective film and for the analysis of the black nickel powder, a Bruker D8-Advance with a Bragg-Brentano geometry was used. Both use monochromatic Cu-Kα radiation (λ = 1.5418 Å). To study the oxidation process at distinct temperatures in the black nickel film and to differentiate from the bright nickel underlayer, the black nickel films were electrodeposited directly on stainless steel at the same conditions as for SS/Ni/NB films. The black nickel film average thickness before and after thermal treatments were 290±10 nm and 260±10 nm respectively, the sampling area was 5 x 10^{-5} m^2. The film thickness was measured with profilometry using a KLA-Tencor D-120. The thickness of the alumina films was 300±10 nm.

Black nickel powder was also analyzed to determine the effects of interaction between the substrate and black nickel under thermal treatment. Black nickel powder was obtained by scraping the material off the SS substrate with electrodeposited black nickel film. The powders were further characterized using differential scanning calorimetry (DSC) using a TA Instruments, Discovery TGA series. The samples were heated in air at temperature range of 25 °C to 500 °C.

Raman spectroscopy measurements were performed at room temperature (25 °C) using 488 nm and 633 nm laser light (1 x 10^{-3} W) in a confocal Raman spectrophotometer (Alpha 300, WiTec) for excitation in a back-scattering geometry. The confocal microscope with a 50X objective on a triple spectrometer was operated in the subtractive mode. It was equipped with a detector illuminated by backlighting; the Raman signal was calibrated with a Si reference. The measurements were performed in three points on each sample, and generally the characteristics observed in each spectrum were independent of location.

The scale-up was achieved by using the experimental conditions for the films obtained on 0.0016 m^2 SS samples and using a steel electrochemical plating cell covered with an anticorrosion ceramic coating of 2 m long, 0.36 m wide, and 0.3 m high. The counter electrodes consisted of nickel rounds in titanium baskets and the current was applied with a power supply. In the case of copper fins, the nickel strike film was not applied. The tube and sheet of the copper fins were welded by ultrasound. The size of the sheet of copper fins was 1.9 m long and 0.107 m wide. The sputtering chamber used for the deposition of alumina on 0.0016 m^2 samples was also used to deposit alumina and AMA coatings on electrodeposited nickel-coated copper fins. The chamber was provided with lateral side arms of 2 m to house the copper fins and contains a system for moving the pieces. Alumina and molybdenum magnetrons of suitable size were used.

3. Results

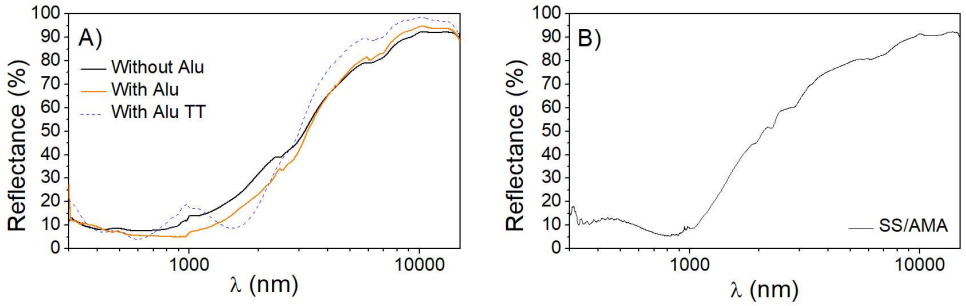

Fig. 1: A) Reflectance spectra for electrodeposited SS/Ni/NB with sputtered alumina with thermal treatment (TT) at 250 °C for 200 hours. B) Reflectance spectrum for SS/AMA.

The Figure 1 A) shows the reflectance spectra for electrodeposited Ni/NB on stainless steel substrates with alumina before and after thermal treatment. In the graph it is possible to observe that the absorptance increased when the alumina was present as shown in Table 2. After the thermal treatment, between 300 nm to 2500 nm some interference peaks appear related with the coupling between the refractive indices of the black nickel and the alumina. The thermal emittance decreased related with the increase of the slope in the infrared range; this could be explained by the recrystallization of the bright nickel interlayer after the thermal treatment. Figure 1 B) shows the reflectance curve for the sputtered AMA coating on stainless steel. The graph for the thermally treated sample at 250 ºC was superimposed with the as-deposited film, showing the thermal stability of this coating at the treatment temperature.

Tab. 2: Optical values calculated with equations 1 and 2 for the deposited selective coatings before and after the thermal treatment.

	α 0.3-2.5 μm (%)	**ε at 250 °C 2.5-15 μm (%)**	**Alumina (Alu) thickness (nm)**	**AMA thickness Alu/Mo/Alu (nm)**	**Spectral selectivity S=α–0.5ε (%)**
SS/Ni/NB	88 ± 1	16 ± 1			80 ± 1.4
SS/Ni/NB	92 ± 1	16 ± 1	300		84 ± 1.4
SS/Ni/NB TT	90 ± 1	10 ± 1	300		85 ± 1.4
SS/AMA	89 ± 1	10 ± 1		90-10-90	84 ± 1.4
SS/AMA TT	89 ± 1	10 ± 1			84 ± 1.4

In the reflectance graph for the thermal treated samples several bands were observed, which can be attributed to interference effects or effects of interdiffusion substrate components towards the absorber film. In order to try to explain the observed changes in reflectance for the films with alumina, DSC measurements were performed. Figure 2 A) shows the DSC measurement for the black nickel powder. From 250 ºC to 300 ºC a shoulder can be observed related with $Ni(OH)_2$ crystallization to NiO. From 342 ºC to 450 ºC another exothermic shoulder can be observed related to Ni oxidation in the black nickel film. The above observations can be correlated with X-ray diffraction results in Figure 2 B). The measurement for the powder that was not treated shows reflections for Ni metal. For the sample treated at 250 ºC, an additional reflection related with NiO is observed. After thermal treatment at 350 ºC the peaks for metallic nickel decrease and the peaks for NiO become more intense.

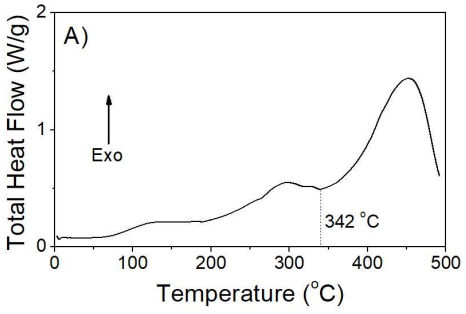

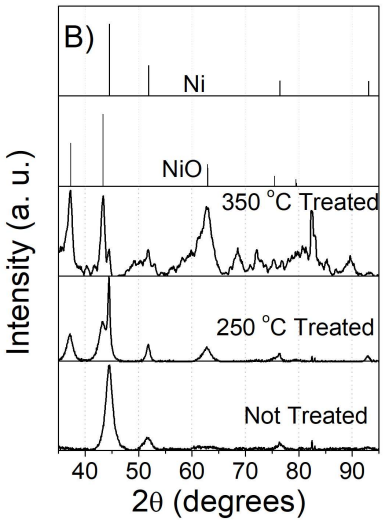

Fig. 2: A) DSC measurements for black nickel powder. B) XRD measurements for black nickel powders obtained from electrodeposited films. The reference pattern for NiO was according to the International Centre for Diffraction Data (ICDD) Powder Diffraction File PDF 073-1559, and for Ni was the PDF pattern 004-0850.

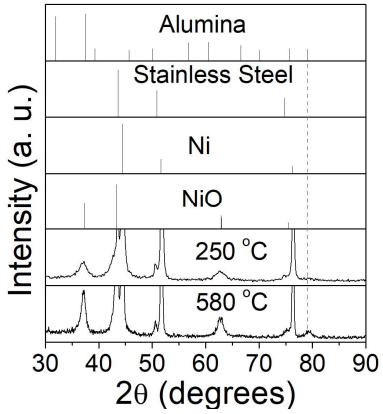

Fig. 3: XRD measurements for SS/Ni/NB with alumina after thermal treatment at 250 °C and 580 °C. Diffraction peaks of stainless steel were found according to the International Centre for Diffraction Data (ICDD) Powder Diffraction File (PDF) PDF 33-0397, The reference pattern for NiO was the PDF 073-1559, for Ni was the PDF pattern 004-0850 and the alumina PDF pattern was 047-7292.

The X-ray diffraction patterns for the SS/Ni/NB/Alu films only show peaks related with bright nickel and stainless steel. The thermally treated samples only show peaks for nickel, stainless steel, and nickel oxide, indicating that the alumina deposited was amorphous and that the thermal treatment at 250 ºC did not crystallize the film. For the sample treated at 580 ºC peaks for alumina were detected indicated with a dotted line in Figure 3.

Figure 4 shows the SEM images of the electrodeposited films before and after thermal treatment. In Figure 4 A) the nanostructured porous morphology of black nickel film is observed; it is formed by nanoflakes vertically oriented to the substrate. In Figure 4 B) it is possible to observe that the nanoflakes are composed of smaller spherical aggregates, but the morphology does not change after thermal treatment. Figure 4 C) shows the morphology of the sample covered with alumina after treatment at 250 ºC: the samples were covered without cracks or voids and the nanoflakes were completely covered with alumina. In the film with 300 nm alumina a homogeneous and compact morphology exists.

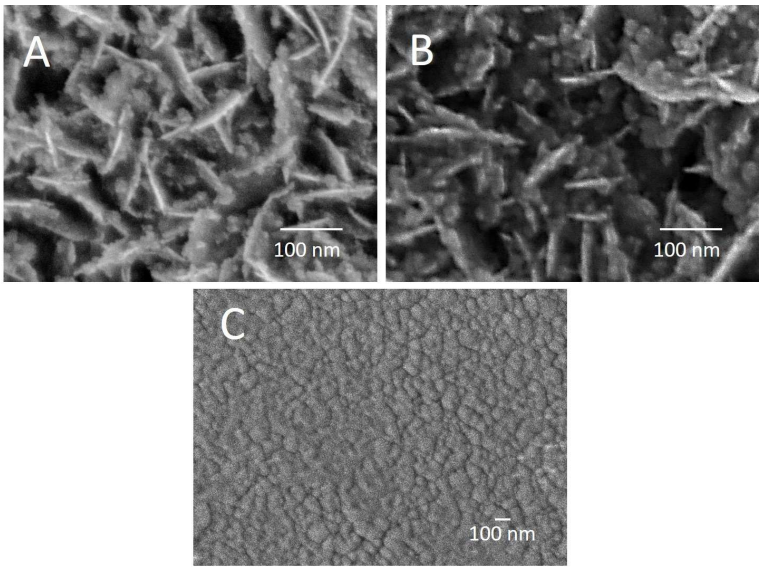

Fig. 4: SEM images for black nickel films: A) without thermal treatment; B) after thermal treatment; and C) alumina film on top of SS/Ni/NB after thermal treatment at 250 ºC.

With the intention to corroborate that after the treatment at 250 ºC the components of the substrate did not diffuse towards the absorber surface; RAMAN measurements were performed. Figure 5 shows the reference spectra of NiO, $Ni(OH)_2$ and NiOOH. The NiO and NiOOH spectra were taken of the RRUFF data base and the $Ni(OH)_2$ spectrum was obtained from an electrodeposited film on stainless steel. From 400 cm^{-1} to 650 cm^{-1} overlapping shoulders can be observed in the two samples, both with and without thermal treatment. For the sample after treatment at 250 ºC, it was found that the shoulders at 1390 cm^{-1} and 1610 cm^{-1} disappear, in concordance with the DSC measurements that showed that at this temperature $Ni(OH)_2$ crystallizes. This measurement emphasizes the thermal stability of the films at this temperature and shows that components from the substrate do not diffuse towards the absorber film.

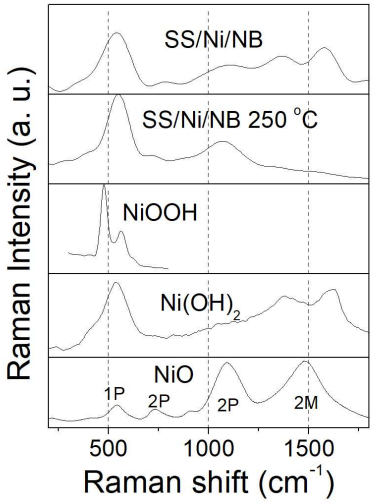

Fig. 5: Raman measurements for black nickel films with and without thermal treatment.

Once the characteristics of black nickel and AMA films were studied on stainless steel, we proceeded to build and evaluate solar collectors with copper fins coated with Ni/NB/Alu, and fins with electrodeposited nickel and sputtered AMA. The collectors were evaluated according the Mexican standard NMX-ES-001-NORMEX-2005 ("NORMA NMX-ES-001-NORMEX-2005, Energía solar – rendimiento térmico y funcionalidad de colectores solares para calentamiento de agua – método de pruebas y etiquetado," 2005).

The stagnation temperature is known to be less than 200 ºC for these devices so the results obtained on stainless steel for SS/Ni/NB/Alu and SS/AMA coatings are representative for these systems on copper. In addition, the stability of selective coatings on copper was previously studied (Estrella-Gutiérrez et al., 2016). We found that at 200 ºC the bright nickel act as diffusive barrier to copper atoms. The performance of the fins was compared with the Cu-TiNOX. The Cu-TiNOX is a benchmark selective coating in the market. The thermal efficiency of built solar collectors with electrodeposited/sputtered fins was calculated from equation 3 where ṁ is the mass flow of water (kg s^{-1}), C is the specific heat of water (4186 J kg^{-1} K^{-1}), G is the solar irradiance (W m^{-2}), A is the collector aperture area (m^2). The results are shown in Table 3.

$$\eta = \frac{\dot{m}C\,(T_{out} - T_{in})}{GA} = \frac{Q_u}{GA} \qquad \text{(eq. 3)}$$

Tab. 3: Results of the characterization of single-fin collectors; the aperture area of the collectors was 0.43 m^2. The transmittance (τ) of the collector glass was 0.85±0.01. A = 0.2 m^2

Fin	T_{in} (ºC)	T_{out} (ºC)	Solar Irradiance (W m^{-2})	ΔT (ºC)	Q_u (W)	η (%)	α (%)	ε (%)	Optical efficiency (ατ)
Cu/Ni/NB/Alu	64.3	67.0	1029.5	2.8	84	40	88.5±0.1	11.2±0.1	0.752
Cu/Ni/AMA	67.2	69.9	864.0	2.6	84	48	89.0±0.1	8.0±0.1	0.756
Cu/TiNOX	63.7	66.5	1013.2	2.8	92	45	92.0±0.1	6.0±0.1	0.782

From Table 3 it can be observed that the performance of the fins with AMA was higher than for the TiNOX fin, and the fin with alumina shows a similar efficiency value. The theorical optical efficiency was calculated as ατ. The results show that the experimental efficiency of the solar collectors is not only a function of the optical properties related with the highest theoretical optical efficiency. Instead, the difference between the trends observed for the optical and experimental efficiencies illustrate that additional factors play a role.

4. Conclusions

Selective coatings obtained by sputtering and electroplating show promising optical properties after thermal treatment, and both processes were scaled-up towards solar collectors. The performance of individual fin collectors with Cu/Ni/BN covered with alumina and the Cu/Ni/AMA coatings was found to be close to the benchmark selective coating. XRD and DSC measurements showed the temperature range of thermal stability of black nickel powder. From the experimental result we can conclude that the use of mixed techniques was promising for the preparation of selective coatings with excellent thermal performance.

5. Acknowledgments

The authors are grateful for the financial support received from the Institute of Renewable Energies (IER-UNAM), through the Mexican Center for Innovation in Solar Energy (CeMIE-Sol), within the framework of the 2013-02 Call, of the CONACYT SECTORIAL FUND -SENER-ENERGY SUSTAINABILITY, within the Strategic Projects 69, 18 and 81, through which it was possible to develop research and support the training of human resources at the postgraduate level. We also gratefully acknowledge the help of Willian Cauich, Beatriz Heredia, Dora Huerta, Daniel Aguilar, and José Bante-Guerra by the characterization of the materials, and the National Laboratory for the Study of Nano and Biomaterials (LANNBIO) for the use of the equipment.

6. References

Abbas, A., 2000. Solchrome solar selective coatings - an effective way for solar water heaters globally. Renew. energy 19, 145–154. https://doi.org/10.1016/S0960-1481(99)00028-2.

Berner, J., 2016. Manufacturers of thin coatings need to have a thick skin. Sun Wind Energy 4, 38–41.

Boström, T., Westin, G., Wäckelgård, E., 2007. Optimization of a solution-chemically derived solar

absorbing spectrally selective surface. Sol. Energy Mater. Sol. Cells 91, 38–43. https://doi.org/10.1016/j.solmat.2006.07.002.

Boström, T.K., Wäckelgård, E., Westin, G., 2004. Anti-reflection coatings for solution-chemically derived nickel - Alumina solar absorbers. Sol. Energy Mater. Sol. Cells 84, 183–191. https://doi.org/10.1016/j.solmat.2003.12.015.

Estrella-Gutiérrez, M.A., Lizama-Tzec, F.I., Arés-Muzio, O., Oskam, G., 2016. Influence of a metallic nickel interlayer on the performance of solar absorber coatings based on black nickel electrodeposited onto copper. Electrochim. Acta 213, 460–468. https://doi.org/10.1016/j.electacta.2016.07.125.

Gogna, P.K., Chopra, K.L., 1979. Selective black nickel coatings on zinc surfaces by chemical conversion. Sol. Energy 23, 405–408. https://doi.org/10.1016/0038-092X(79)90148-8.

Khatibani, A.B., Rozati, S.M., 2016. Spray pyrolytically grown NiAlOx cermets for solar thermal selective absorbers: Spectral properties and thermal stability. Bull. Mater. Sci. 39, 97–107. https://doi.org/10.1007/s12034-015-1146-y.

Lizama-Tzec, F.I., Macías, J.D., Estrella-Gutiérrez, M.A., Cahue-López, A.C., Arés, O., de Coss, R., Alvarado-Gil, J.J., Oskam, G., 2014. Electrodeposition and characterization of nanostructured black nickel selective absorber coatings for solarthermal energy conversion. J. Mater. Sci. Mater. Electron. https://doi.org/10.1007/s10854-014-2195-5

Manson, J.J., Brendel, T.A., 1982. Maxorb -a new selective surface on nickel. SPIE 324, 139–145.

NORMA NMX-ES-001-NORMEX-2005, Energía solar – rendimiento térmico y funcionalidad de colectores solares para calentamiento de agua – método de pruebas y etiquetado, 2005. . Secr. Energ. 1–65.

Nunes, R.A.X., Costa, V.C., Sade, W., Araújo, F.R., Silvaa, G.M., 2018. Selective surfaces of black chromium for use in solar absorbers. Mater. Res. 21. https://doi.org/10.1590/1980-5373-mr-2017-0556.

Patel, S.N., Inal, O.T., Singh, A.J., Scherer, A., 1985. Optimization and thermal degradation study of black nickel solar collector coatings. Sol. Energy Mater. 11, 381–399. https://doi.org/10.1016/0165-1633(85)90010-3

Shimadzu Corporation, 2013. C101-E127 UV Talk Letter 12, 1–12.

Wackelgard, Ewa; Hultmark, G., 1998. Industrially sputtered solar absorber surface. Sol. Energy Mater. Sol. Cells 54, 165–170. https://doi.org/DOI: 10.1016/S0927-0248(98)00067-1.

Wäckelgard, E., 1998. Characterization of black nickel solar absorber coatings electroplated in a nickel chlorine aqueous solution. Sol. Enegy Mater. Sol. Cells 56, 35–44.